Nanoscale

Accepted Manuscript

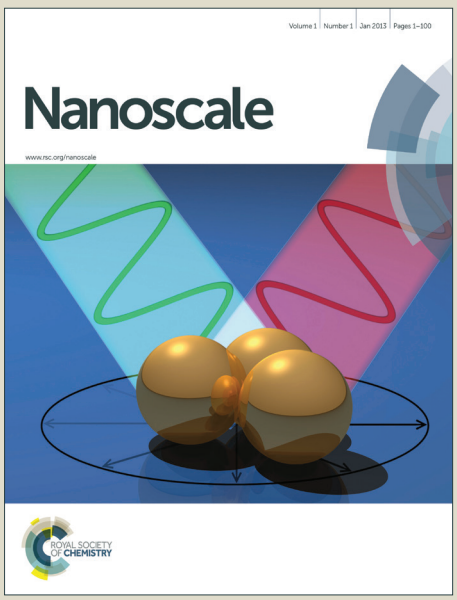

ROYAL SOCIETY OF CHEMISTRY

www.rsc.org/nanoscale

PSMA-mediated endosome escape-accelerating polymeric micelles for targeted therapy of prostate cancer and real time tracing their intracellular trafficking

Yajie Gao[a], Yanfang Li[b], Yushu Li[a], Lan Yuan[c], Yanxia Zhou[a], Jinwen Li[a], Lei Zhao[a], Chao Zhang[a], Xinru Li[a,**] and Yan Liu[a,*]

[a] *Department of Pharmaceutics, School of Pharmaceutical Sciences, Peking University, Beijing 100191, China*

[b] *Central Lab, Peking University Third Hospital, Beijing 100191, China*

[c] *Medical and Healthy Analytical Center, Peking University, Beijing 100191, China*

*Corresponding author. Phone: 86-10-82801508

**Corresponding author. Phone: 86-10-82801508

E-mail: yanliu@bjmu.edu.cn, ll@bjmu.edu.cn

Abstract Cytotoxicity of chemotherapeutic agents to healthy organs and drug resistance of tumor cells are believed to be main obstacles to the successful cancer chemotherapy in clinic. To ensure that anticancer drugs could be delivered to tumor region, quickly released from carriers in tumor cells and rapidly escape from endo/lysosomes, YPSMA-1-modified pH-sensitive polymeric micelles, that would be advantageous in recognizing prostate specific membrane antigen (PSMA), were designed and fabricated to targeted delivery of paclitaxel to tumors based on pH-sensitive diblock copolymer poly(2-ethyl-2-oxazoline)-poly(D,L-lactide) (PEOz-PLA) and YPSMA-1-PEOz-PLA for treating prostate cancer. HOOC-PEOz-PLA with critical micelle concentration of 5.0 mg/L was synthesized and characterized by ^{1}H NMR and gel permeation chromatography. The prepared YPSMA-1-modified micelles with about 30 nm in diameter exhibited rapid release behavior at endo/lysosome pH and favorable ability of fast endo/lysosome escape observed by confocal microscopy. More importantly, we evidenced for the first time that both endosome and lysosome escape existed for pH-sensitive micelles via real time tracing using confocal microscopy and the real time endo/lysosome escape process was presented. The YPSMA-1-modified micelles were very effective in enhancing the cytotoxicity by increasing the cellular uptake in PSMA-positive 22Rv1 cells, which was verified the correlation with PSMA expression in tumor cells by flow cytometric analysis and confocal microscopy. Moreover, the active targeting and pH-sensitivity endowed YPSMA-1-modified micelles with higher antitumor efficacy and negligible systemic toxicity in 22Rv1 xenograft-bearing nude mice compared with unmodified micelles and Taxol®. These results suggested that the application of combining YPSMA-1 modification with

pH-sensitivity to polymeric micelles may be an approach in the efficient delivery of anticancer drugs for treating PSMA-positive prostate cancers.

Keywords: endo/lysosome pH-responsive polymeric micelles; paclitaxel; PSMA; tumor-targeting; endosome escape; prostate cancer therapy

1 Introduction

Currently, prostate cancer is one of the most frequently diagnosed malignant diseases and the second leading cause of death in men. The first choice of treatment of prostate cancer is androgen ablation therapy followed by chemotherapy with drugs such as paclitaxel and docetaxel. However, the benefit of chemotherapy is limited due to its serious systemic toxicity. To ameliorate this challenge, different types of nanocarriers have been developed for delivery of antitumor drugs, with polymeric micelles being by far the most extensively used and studied.[1, 2] Polymeric micelles have presented great potential in improved water solubility of anticancer drugs, prolonged blood circulation time, and higher accumulation at tumor site by the enhanced permeability and retention (EPR) effect.[3] However, the efficiency of passive targeting to tumor by EPR effect is limited. The nonspecific distribution of anticancer drugs may result in toxicity to health organs.[4] Hence, recognition and uptake of micelle delivery system by tumor cells remain a considerable challenge.[5-8]

The decoration of nanocarrier surface with various ligands has been demonstrated to promote targeted delivery of drugs to tumor sites and improve the cellular uptake. These ligands are recognized by their specific receptors/antigens on tumor cell surface through

specific interactions.[9] Here, we focused on anti-PSMA (prostate specific membrane antigen) antibody YPSMA-1 as a candidate decoration. PSMA, a classic type-II glycosylated transmembrane protein, is overexpressed in primary and metastatic prostate cancer cells and the tumor neovasculature.[10-12] Its expression is independent of androgen, and upregulated after chemotherapeutics or surgical ablation therapy [13] and with disease progression.[14] Several studies demonstrated that YPSMA-1-modified vehicles, such as liposomes,[11, 15] could efficiently home to PSMA-expressing tumor cells and xenografts, and enhance therapeutic efficacy.

Notably, a great concern is that slow release of anticancer drug from polymeric micelles in tumor cells may result in lower level of intracellular free drug and thereby limited antitumor efficacy.[1, 16] Even worse, maintaining a lower level of intracellular free drug for a long time may lead to occurrence of drug resistance for tumor cells. Consequently, to guarantee the delivery of anticancer drug to tumor site and sufficient drug concentration for optimal efficacy and reduce side effects, polymeric micelles are required to remain stable in the blood circulation and rapid release drugs to cytoplasm in tumor cells. This might be achieved by using targeted polymeric micelles with a triggered release mechanism which enables the nanocarriers to release their cargos in response to the stimuli of tumor intracellular compartment, such as pH or enzymes.[17, 18] On the other hand, ligand-modified nanocarriers are generally entrapped in endosomes after being internalized into tumor cells via an endocytic pathway, and finally delivered into acidic lysosomes, thereby leading to an inferior antitumor efficacy due to the degradation of the cargos by the lysosomal enzymes.[19] Therefore, it is very important to facilitate drug

escape from endo/lysosomal vesicles.[20, 21] pH-responsive polymeric micelles appeared to be the most attractive candidate due to the fact that the internalized micelles experienced a pH gradient from 5.5-6.5 in endosomes to 4.5-5.0 in lysosomes in their intracellular trafficking pathway.

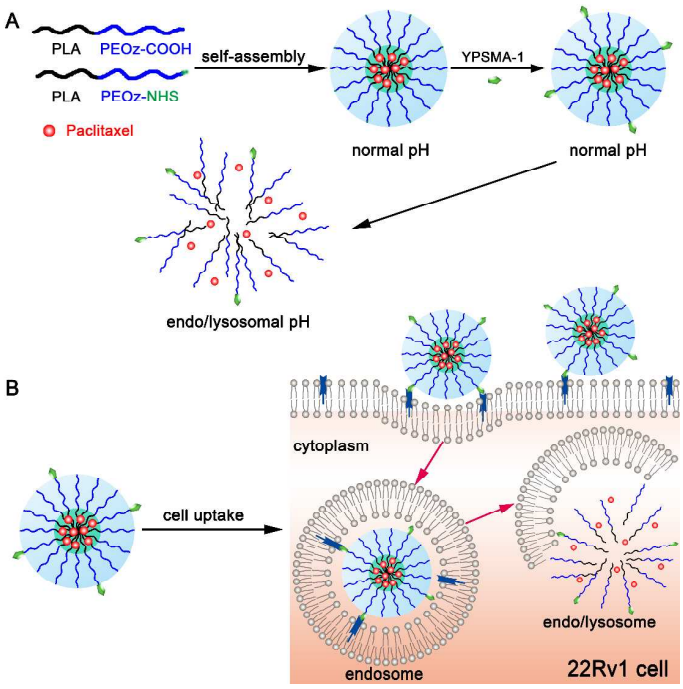

Scheme 1 (A) Schematic illustration of multifunctional polymeric micelles modified with YPSMA-1 and the acid-triggered drug release from the pH-sensitive micelles. (B) Schematic illustration of cellular uptake and intracellular trafficking of YPSMA-1-modified PEOz-PLA polymeric micelles in tumor cells.

In order to integrate the merits of ligand-modified polymeric micelles for enhanced accumulation at tumor site and promoted uptake by tumor cells, and pH-sensitive polymeric micelles for quick drug release in tumor cells and efficient endo/lysosomal escape, we designed ligand-modified pH-sensitive polymeric micelles based on pH-sensitive diblock copolymer poly(2-ethyl-2-oxazoline)-poly(D,L-lactide) (PEOz-PLA)

and YPSMA-1-PEOz-PLA. A schematic diagram depicting the formation of multifunctional micelles and the intracellular trafficking was shown in Scheme 1. We hypothesized that the micelles would be endued with tumor cell-targeting ability and pH-response to intracellular compartments. Therefore, the physicochemical properties, pH-dependent *in vitro* release, and *in vitro* cytotoxicity against PSMA-negative PC-3 and PSMA-positive 22Rv1 cells and cellular uptake as well as real-time intracellular trafficking of micelles were all investigated in detail. Moreover, the competitive inhibition effect of free YPSMA-1 was examined. The potency of this smart delivery system in tumor therapy was evaluated in PC-3 and 22Rv1 tumor-bearing mice. The designed micelles were expected to be an effective delivery system for anticancer drugs to treat prostate cancers.

2 Experimental section

2.1 Materials

Paclitaxel was purchased from Guilin Huiang Biopharmaceutical Co. Ltd. (Guilin, China). YPSMA-1 was provided by Abcam (Cambridge, UK). 2-ethyl-2-oxazoline supplied by Sigma-Aldrich (St Louis, MO, USA) was dried by vacuum distillation over calcium hydride. D,L-lactide was obtained from Daigang Biological Technology Co. Ltd. (Jinan, China) was purified by recrystallization from ethyl acetate. Ethyl 3-bromopropionate and stannous octoate were products of Aladdin reagent company (Shanghai, China). N-hydroxysuccinimide (NHS) and N-(3-dimethylaminopropyl)-N'-ethylcarbodiimide hydrochloride (EDC·HCl) were supplied by J&K scientific Ltd. (Beijing, China). Sulforhodamine B sodium salt (SRB) and coumarin-6 (donated as C6) were purchased from Sigma-Aldrich (St Louis, MO, USA). mPEG5000-PLA5000 was synthesized by our

laboratory as reported previously.[22] Bis Benzimide Hoechst 33258 was obtained from Biodee Biotechnology Co. Ltd. (Beijing, China). LysoTracker® Red, CellLight® Endosomes-RFP and CellLight® Lysosomes-RFP were purchased from Life Technologies (Gaithersburg, MD, USA). 3,3-dioctadecyl oxacarbocyanine perchlorate (DiO) and 1,1-dioctadecyl-3,3,30,30-tetramethylindocarbocyanine perchlorate (DiI) were purchased from J&K Chemical Ltd. (Shanghai, China).

2.2 Synthesis and characterization of polymers

2.2.1 Synthesis of HOOC-PEOz-PLA

HOOC-PEOz-PLA diblock copolymer was synthesized using a two-step reaction procedure (Scheme 2A). HOOC-PEOz-OH was first synthesized by cationic ring-opening polymerization of 2-ethyl-2-oxazoline (25 g) using ethyl 3-bromopropionate (0.5 g) with 1.1 equiv of KI as initiators at 100°C for 24 h in acetonitrile (50 mL) under nitrogen atmosphere and then using 2.5 equiv of methanolic KOH as terminator followed by stirring at 80°C for 12 h.[23] The solvent was then removed from the reaction mixture by rotary evaporation. The crude product was dissolved in dichloromethane and precipitated in cold diethyl ether, and further purified by dialysis with a dialysis membrane (MWCO 3500, Millipore Co. Ltd, USA) against deionized water for 48h. The dialysis solution was subsequently lyophilized to obtain the solid of HOOC-PEOz-OH with white color.

The resulting HOOC-PEOz-OH was subsequently polymerized with D,L-lactide in toluene at 160°C for 36h using stannous octoate as the catalyst.[24] The product was then obtained by precipitating in cold diethyl ether and drying under vacuum.

The polymers were characterized by ^{1}H NMR and gel permeation chromatography

(GPC). The obtained polymers were dissolved in $CDCl_3$ and then ^1H NMR spectra were recorded on a Bruker MSL2300 spectrometer (400 MHz, Germany) using tetramethylsilane (TMS) as an internal reference at room temperature to characterize the chemical structure of the products. The molecular weight and molecular weight distribution were measured by GPC (Waters 1515) with a refractive index detector (Waters 2414) by using polystyrene as standards.

2.2.2 Synthesis of NHS-PEOz-PLA

HOOC-PEOz-PLA, EDC·HCl (2 excess), NHS (2excess) and dichloromethane were added to a round-bottle flask equipped a magnetic stirring bar, purged with nitrogen atmosphere (Scheme 2B). The reaction was maintained for 24 h at room temperature. The reaction mixture was washed twice with saturated NaCl solution to remove the excessive NHS and EDC·HCl, then precipitated in cold diethyl ether and dried in vacuum to constant weight. The final product was characterized via ^1H-NMR.

2.3 Determination of critical micelle concentration of HOOC-PEOz-PLA

The critical micelle concentration (CMC) of the copolymer was measured by a fluorescence technique with pyrene as a hydrophobic probe as described previously.[25]

2.4 Preparation of drug-loaded polymeric micelles

Paclitaxel (PTX)-loaded polymeric micelles (denoted as PTX/PM) were prepared by thin-film hydration method.[22] Briefly, HOOC-PEOz-PLA (10 mg) and paclitaxel (1 mg) were dissolved in 20 mL of methanol followed by evaporation under vacuum at 60 °C to form a stripped film. The resultant thin film was hydrated with 5 mL of deionized water at 60°C and then vortexed for 5 min. Non-encapsulated paclitaxel was removed by filtration

of the micelle suspensions through a 0.22 μm polycarbonate membrane (Millex-GV, Millipore, USA) to obtain a clear and homogeneous micelle solution.

For preparation of PTX-loaded polymeric micelles modified with YPSMA-1 (denoted as PTX/PM-Y) (Scheme 1A), NHS-PEOz-PLA, HOOC-PEOz-PLA and PTX (5:5:1, w/w/w) were dissolved in methanol, and then evaporated, hydrated, vortexed and filtered as described above to obtain N-hydroxysuccinimide-activated PTX/PM. The resultant micelle suspension was subsequently allowed to react with YPSMA-1 for 24 h under magnetic stirring. After which, the micelle suspension was subjected to a Sepharose CL-4B column and eluted with distilled water to remove the free YPSMA-1. The conjugation efficiency of YPSMA-1 was about 25.1% determined using the Micro BCA Protein kit.

C6-, DiI/DiO-loaded polymeric micelles were prepared as described above. In the C6-loaded micelles, the C6/polymer ratio was 1:1000 (w/w); while in the (DiI/DiO)-loaded micelles (denoted as FRET micelles), the DiO/polymer and DiI/polymer ratio was 1:500 (w/w), respectively.

2.5 Physicochemical characterization of polymeric micelles

Size and size distribution (polydispersity index, PDI), and zeta potential of polymeric micelles were determined by dynamic light scattering (DLS) using Malvern Zetasizer Nano ZS (Malvern, UK) with a scattering angle of 90° at 25°C after diluting the micelle solution to an appropriate volume with deionized water.

The morphology of micelles was visualized by transmission electron microscope (TEM, JEM-1230, JEOL, Japan). Before examination, the sample was stained with a drop of 1 wt% phosphotungstic acid solution, and then placed on a copper grid with carbon film

followed by removal of the excess fluid with filter paper, and dried for 48 h.

The encapsulation efficiency (EE) and loading content (LC) were determined as previously reported. [26] The PTX level loaded in micelles was measured by HPLC method. [26] Similarly, the amount of C6 or DiI/DiO loaded in micelles was determined by fluorescence spectrophotometry.

To evaluate the stability of the prepared micelles, a sample of PTX/PM solution in phosphate buffered saline (PBS, pH7.4) was stored at 25°C. Changes in the micelle size and PDI, and EE were examined as described above.

The *in vitro* release behavior of PTX from various PTX-loaded micelles was monitored by using a dialysis-bag diffusion method as previously described with little modification.[26] Briefly, 1mL of PTX-loaded micelle solution was introduced into a dialysis bag (MWCO 3500), and the sealed dialysis bag was completely submerged into 50 mL of PBS (pH5.0, 7.4) with 0.5% Tween 80 at 37°C and 100 rpm. At predetermined time points (1, 4, 8, 12, 24h), 1 mL of the release medium was withdrawn and replaced with equal volume of fresh media. The concentration of released PTX in medium was measured by HPLC method as described above and the accumulative release amount (%) was calculated.

The *in vitro* leakage of C6 from polymeric micelles in serum-free medium (pH 7.4) under continuous gentle shaking at 37°C (100 rpm) was evaluated using a dialysis diffusion method as described above. The cut-off molecular weight of the dialysis bag was 3500 Da.

2.6 Cell culture

PC-3 and 22Rv1 cells were obtained from Cell Culture Center of Institute of Basic Medical Sciences, Chinese Academy of Medical Sciences and Peking Union Medical College (Beijing, China). Cells were cultured in RPMI 1640 medium (MAC Gene Technology) supplemented with 10% fetal bovine serum (FBS, Gibco) and 1% Penicillin-Streptomycin in 5% CO_2 humidified atmosphere at 37°C.

2.7 Stability of polymeric micelles after contacting with cells

The stability of the micelles was evaluated through the release of core-loaded molecules from micelles by using the Förster resonance energy transfer (FRET) method when they were in contact with 22Rv1 cells.[27] Briefly, 22Rv1 cells were seeded on a glass bottom culture dish (35-mm dish with 20-mm glass bottom well) and cultured at 37°C under 5% CO_2 for adherence. After the cells were subcultivated at 80-90% confluence, the culture media were removed, and the cells were washed with serum-free medium at 37°C for three times. Subsequently, the medium containing FRET micelles (final concentration of both DiI and DiO was 4 μg/mL) was added. After 1 h incubation, the cells were washed with cooled PBS for three times and fixed with 4% paraformaldehyde at 37°C for 15 min followed by washing thrice with PBS. FRET images were obtained with a confocal laser scanning microscope (CLSM, TCS SP5, Leica, Germany). The excitation and emission wavelengths for DiO were 484 nm and 500-530 nm, respectively, and 549 nm and 555-655 nm for DiI, respectively. For determination of FRET, the excitation wavelength (484 nm) of DiO as the donor and the emission wavelength (555-655 nm) of DiI as the acceptor were used, respectively.

2.8 Cytotoxicity assessment

The SRB assay was applied to investigate the *in vitro* cytotoxicity of various PTX-loaded micelles on PC-3 and 22Rv1 cells.[24, 28] In brief, PC-3 or 22Rv1 cells were seeded in 96-well plates at a density of 1×10^4 cells/well and cultured at 37°C in 5% CO_2 humidified atmosphere for 24 h. Then the culture medium in each well was replaced with 200 μL of fresh medium containing free PTX, different micelle formulations with serial PTX concentration, respectively. The PTX-free culture medium was used as negative control. Cells were also treated with blank micelles with indicated HOOC-PEOz-PLA concentrations to evaluate the cytotoxicity of the vehicle. After incubation for further 72h, cells were washed with cold PBS for three times and fixed with 200 μL of 10% trichloroacetic acid (TCA) for 1h at 4°C, then washed 5 times with deionized water after removing TCA and dried in the air. The fixed cells were then stained with 100 μL of 0.4% SRB for 30 min and followed by washing 5 times with 1% acetic acid after removing SRB and drying at 37°C. The absorbance at 540 nm was determined using a microplate reader (BIO-RAD model 680, Shanghai, China) after the bound dye in each well was dissolved in 200 μL of 10 mM Tris. The cytotoxicity of tested samples was expressed as the ratio of the absorbance of the tested groups to that of the negative control.

2.9 Cellular uptake assay

2.9.1 Flow cytometric analysis

PC-3 or 22Rv1 cells were seeded into 6-well plates (3×10^5 cells/well) and cultured for 24 h at 37°C under 5% CO_2. The medium was replaced by the medium containing free C6, C6/PM, and C6/PM-Y with a final C6 concentration of 100 ng/mL. After 4 h incubation, the cells were washed thrice with cold PBS, trypsinized and harvested with 0.4 mL of 0.2%

(w/v) trypsin-0.1% (w/v) EDTA solution, and resuspended in 0.5 mL of PBS followed by filtration through a nylon mesh. The C6 uptake in the cells was measured by FAScan flow cytometer (Becton Dickinson FACSCalibur, Mountain View, USA).

To investigate whether YPSMA-1 could hinder C6/PM-Y endocytosis, cells were pre-incubated with 0.1 μg/mL of free YPSMA-1 for 30 min before they were exposed to C6/PM-Y.

2.9.2 Confocal microscopy observation

PC-3 or 22Rv1 cells were cultured in glass-bottomed 24-well plates at a density of 1×10^5 cells/well for 24 h. The medium was replaced by the medium containing free C6, C6/PM, and C6/PM-Y with a final C6 concentration of 50 ng/mL, respectively. After another 1 h or 1.5 h incubation, the medium was removed and cells were washed thrice with cold PBS followed by fixing with 4% paraformaldehyde at 37°C for 20 min and washing thrice with PBS. Then the fixed cells were stained with Hoechst 33258 for 15 min. The fluorescent images of the cells were visualized using confocal laser scanning microscope (CLSM, Leica, TCS SP2, Germany).

2.10 Tracking of endo/lysosome escape

The endo/lysosomal release of our prepared micelles in PC-3 cells was tracked using CLSM. In order to facilitate the observation of intracellular distribution, the green fluorescence probe C6 was encapsulated into the interior of the micelles to track the intracellular transport pathway. In brief, PC-3 cells were seeded in chambered coverslips and cultured for 24h at 37°C under 5% CO_2. After the culture media were removed, LysoTracker® red (a final concentration of 200 nM) was added. After 30 min incubation,

the cells were washed thrice with PBS. Then the medium containing C6/PM or C6-loaded mPEG-PLA micelles was added with a final C6 concentration of 50 ng/mL. Following incubation for 30 min, the medium was removed and the cells were rinsed thrice with serum-free medium. After an additional 0.5 h, 1h and 3 h of incubation in complete medium, respectively, the cells were washed, fixed and observed using CLSM. The colocalization efficiency was quantitatively analyzed using Pearson's correlation and the CLSM software. The value of Pearson's correlation ranges from -1.0 to 1.0. In general, when the correlation is higher than 0.5, it can be considered the existence of colocalization phenomenon. The closer to 1 indicates the more significant colocalization.[29]

2.11 Real-time imaging of intracellular trafficking process of micelles

The intracellular trafficking process of our prepared pH-sensitive micelles in PC-3 cells was observed intuitively using live-cell time-lapse fluorescence imaging with CLSM. Briefly, PC-3 cells were seeded into 35-mm coverslips-bottom dishes and cultured at 37°C under 5% CO_2 for adherence. The cells were then incubated with CellLight® Endosome-RFP or CellLight® Lysosome-RFP for 24 h to label endosomes and lysosomes, respectively. Following the transfection, cells were washed three times with RPMI 1640 medium, and refreshed with 2 mL of the medium and immediately put on the microscope stage of CLSM. Before imaging, 50 μL C6/PM were added (final amount of C6 was 200 ng). Time-lapse fluorescence images were collected with 30 s intervals to observe endocytosis trafficking process or with 1 min intervals to investigate micelles escape from endosomes or lysosomes. Before observation of the escape behavior from corresponding organelles, the micelles were removed and equal volume of serum-free medium was

supplemented.

2.12 Animals and tumor models establishment

Normal male BALB/c nude mice (6-8 weeks old) were obtained from Animals Center of Peking University Health Science Center. All care and handling of animals were performed with the approval of Institutional Authority for Laboratory Animal Care of Peking University. PC-3 or 22Rv1 cells suspension (0.2 mL, 2×10^6 cells) was injected subcutaneously into the right flank region of the mice. Thereafter, all the treated nude mice were observed every day to monitor the size of tumors by using a digital caliper. The tumor volume was calculated as (tumor length)×(tumor width)^2/2.

2.13 In vivo anti-prostate cancer efficacy

To assess antitumor efficacy, the tumor bearing nude mice were randomly assigned to four groups (n=6) when the tumor volume reached about 100 mm^3 for PC-3 tumors and 50 mm^3 for 22Rv1 tumors, respectively, and received intravenous injection of PTX/PM, PTX/PM-Y, Taxol® and physiological saline via tail vein at a dose of 15 mg PTX/kg body weight at 2-3 day intervals for a total of four treatments, respectively. Body weight and tumor size were measured once every two days throughout the post-exposure period. Solid tumors were collected and imaged.

2.14 Statistical analysis

Data are presented as mean ± standard deviation. One-way analysis of variance was used to determine the statistical significance of differences among multiple groups. A p-value of 0.05 or less was considered to be statistically significant.

3 Results

3.1 Synthesis and characterization of HOOC-PEOz-PLA

As shown in Scheme 2A, HOOC-PEOz-OH was first synthesized by cationic ring-opening polymerization of EOz. The successful synthesis of HOOC-PEOz-OH was verified by ^{1}H NMR spectrum (Fig.1A). The pendent peaks at 1.12 ppm and 2.44 ppm were attributed to methyl (***CH*$_3$**CH_2CO-) and methylene (CH_3***CH*$_2$**CO-) protons in side chains, respectively. The peak at 3.49 ppm was assigned to methylene protons (-N***CH*$_2$*CH*$_2$**N-) in the backbone. The molecular weight (M_n) and molecular weight distribution of HOOC-PEOz-OH determined by GPC was 4338 with relatively low PDI of 1.16.

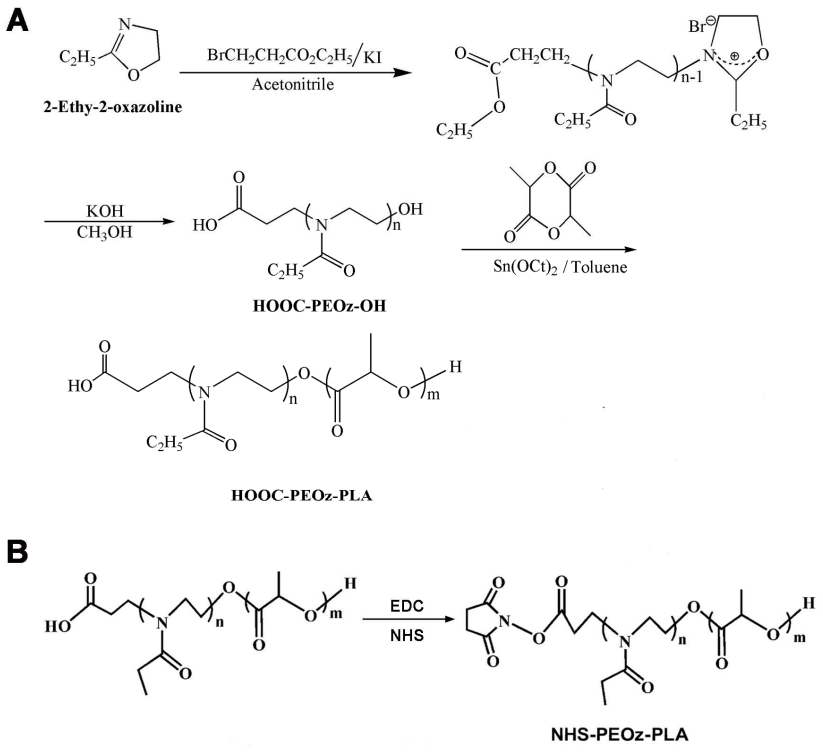

Scheme 2 Synthesis routes of HOOC-PEOz-PLA (A) and NHS-PEOz-PLA (B).

Then, HOOC-PEOz-PLA was synthesized by anionic ring-opening polymerization of HOOC-PEOz-OH and D,L-lactide using stannous octoate as the catalyst (Scheme 2A).

The characteristic peaks corresponding to PLA (5.17 ppm and 1.56 ppm) and PEOz (1.12 ppm, 2.44 ppm and 3.49 ppm) were observed (Fig. 1B), which were in agreement with our previous report.[24] The molecular weight (M_n) of HOOC-PEOz-PLA determined by GPC was 7097 (PDI: 1.26).

The synthesized HOOC-PEOz-PLA exhibited a low CMC of 5.0 mg/L, indicating that the micelles formed by HOOC-PEOz-PLA might provide relatively high stability in systemic circulation as drug delivery carriers.

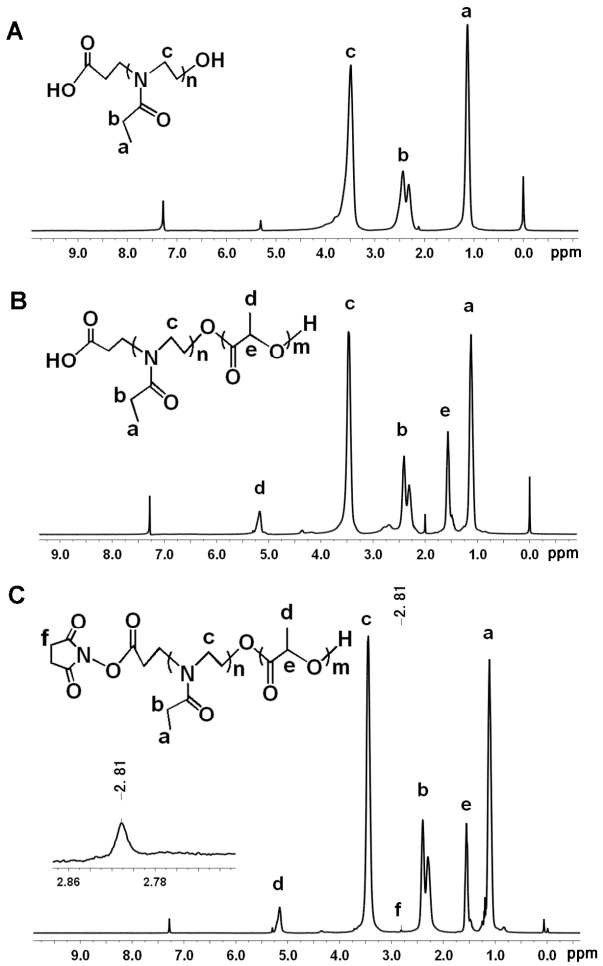

Fig.1 ^{1}H NMR spectrum of HOOC-PEOz-OH (A), HOOC-PEOz-PLA (B) and NHS-PEOz-PLA (C) in $CDCl_3$.

3.2 Synthesis and characterization of NHS-PEOz-PLA

In order to conjugate YPSMA-1 with HOOC-PEOz-PLA, HOOC-PEOz-PLA copolymer was activated with NHS (Scheme 2B). The activation was then confirmed by ^{1}H NMR (Fig.1C). The presence of the characteristic resonances of NHS at 2.81 ppm indicated the successful conjugation of NHS to the terminal of HOOC-PEOz-PLA.

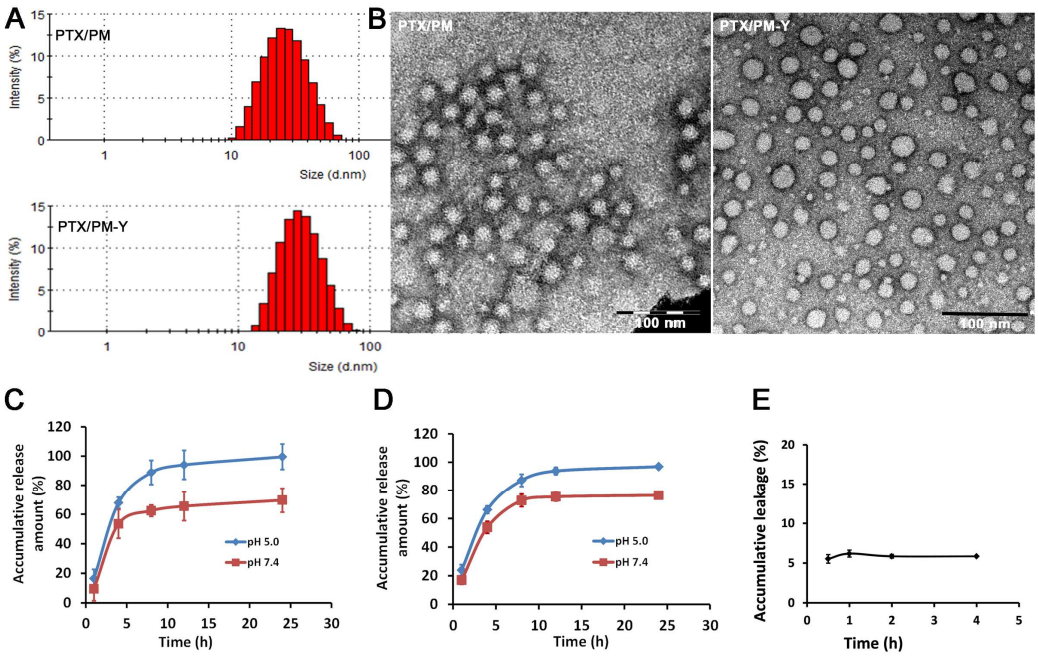

Fig.2 (A) Size distribution of PTX/PM and PTX/PM-Y. (B) Morphological characteristics of PTX/PM and PTX/PM-Y observed by TEM. (C and D) The change of size, size distribution (C) and encapsulation efficiency (D) of micelles as a function of time in PBS at 25°C. (C and D) *In vitro* release profiles of PTX from PTX/PM (C) and PTX/PM-Y (D) at 37°C (*n*=3). (E) *In vitro* leakage of C6 from PEOz-PLA micelles in serum-free medium for 4 h at 37°C (*n*=3).

Table 1 Physicochemical characteristics of blank micelles and various drug-loaded micelles (*n*=3).

Polymeric micelles	Diameter (nm)	PDI	Zeta Potential (mV)	EE (%)	LC (%)
Blank micelles	24.56±0.92	0.15±0.01	---	---	---
PTX/PM	28.30±0.88	0.21±0.01	-8.96±0.20	98.78±1.00	8.98±0.09
PTX/PM-Y	29.94±1.40	0.26±0.03	-2.03±0.66	91.63±0.98	8.33±0.09
C6/PM	34.94±0.35	0.22±0.01	---	84.32±3.63	---
C6/PM-Y	37.29±0.37	0.25±0.01	---	81.43±3.98	---

3.3 Characterization of polymeric micelles

The physicochemical characteristics of nanoparticles play an important role in determining their fate after administration.[30] As listed in Table 1, the synthesized HOOC-PEOz-PLA could self-assemble into micelles with a small average diameter of about 24 nm (blank micelles) and a narrow distribution determined by DLS. A slightly appreciable increase in size for all the PTX-loaded micelles in comparison with blank micelles (Fig. 2A and Table 1) was observed, implying a favorable stability of the nanocarriers. Furthermore, PTX/PM-Y was comparable to PTX/PM in size, indicating that the YPSMA-1 conjugation did not affect the size of the micelles. Importantly, these micelles was beneficial for passively targeted delivery of drugs to tumors due to the fact that they were small enough to penetrate through the leaky vasculatures at tumor site through EPR effect,[31,32] while reducing reticuloendothelial system (RES)-mediated clearance, and big enough to avoid renal filtration.[30] Fig.2B showed the morphological

characteristics of the micelles observed by TEM. It was clearly seen that the micelles were spherical or spheroid in shape, and the sizes were in agreement with the results of DLS measurements. In addition, all PTX-loaded micelles exhibited a negative Zeta potential (Table 1), which might be attributed to the carboxyl groups on the micelle surface, and displayed higher drug encapsulation efficiency (EE) of >91% and loading content (LC) of >8.3%, respectively, which are crucial for their clinical application.

Stability is a very important property of micelles to understand *in vitro* drug uptake and *in vivo* absorption, thereby the micelle size and EE was monitored at different times at room temperature. Within 24 h, the micelles did not show a significant change in size and size distribution (PDI), indicating that the micelles had considerably high thermodynamic stability without aggregation. By contrast, the reduction (about 10.5%) in EE was more profound in the first 4h, then the EE remained constant (about 85%). These suggested that the prepared micelles exhibited favorable stability to a certain extent in physiological condition before reaching targeting sites, which was in agreement with our previous report.[26]

The *in vitro* release of PTX from various polymeric micelles at 37°C was evaluated using a dialysis method at pH 7.4 that mimics the blood environment. Moreover, the release profiles of PTX-loaded micelles under endo/lysosome mimetic circumstances (pH 5.0) were also investigated, since the delivery system would be trapped inside the endo/lysosomes after being endocytosed by tumor cells. As anticipated, the release of PTX from the micelles was pH-dependent. As presented in Fig.2C and Fig.2D, PTX showed a significantly slower release for all micelles at pH 7.4, and about 70% of PTX

was leaked from the micelles within 24 h, while the release of PTX was accelerated at pH 5.0, and almost 100% release was observed within 24 h. Specifically, at 8 h, the release of PTX from two kinds of micelles was suppressed at pH 7.4 and the release profile reached a plateau with accumulative release of approximately 62.4% and 72.7% for PTX/PM and PTX/PM-Y, respectively. In comparison, at pH 5.0, the release of PTX burst to approximately 88.8% and 87.1% at 8 h, respectively, and the release was sustained thereafter. This release behavior of polymeric micelles in the case of our experiment was highly advantageous to targeted cancer therapy due to the fact that the amount of drug released prematurely might be significantly minimized during circulation in the bloodstream, thereby providing an enough amount of drug to effectively kill the cancer cells once the micelles were internalized via endocytosis.

To study the cellular uptake, intracellular distribution and intracellular trafficking pathway of our prepared micelles, a poorly water-soluble fluorescent probe C6 was loaded. As shown in Table 1, the encapsulation efficiencies were all higher than 81%. The leakage profile of C6 from the representative micelles C6/PM in serum-free medium was shown in Fig. 2E. Up to 4 h, the leakage of C6 was less than 5.9% in total. These implied that the leaked C6 before the micelles contacted with the cells was negligible, and the behavior of C6 could represent the micelles.

3.4 Micelle stability analysis after contacting with cells

FRET method was used to detect whether the core-loaded lipophilic agent is still encapsulated in the core of micelles when the micelles are in contact with cells. A FRET pair DiI/DiO was physically loaded into the inner core of PEOz-PLA micelles (denoted as

FRET micelles) with an average diameter of 41.72±0.72 nm measured by DLS. If the FRET pair is located in the inner core of micelles, DiO is excited at a wavelength of 484 nm, the DiI will emit fluorescence at 565 nm. That is to say, FRET occurs due to the close proximity (<10 nm) of DiI and DiO. Upon release of the FRET pair from micelles, the distance between the FRET pair increased (>10 nm), resulting in decreased emission at 565 nm and increased emission at 501 nm.[27] As shown in Fig.3A, a strong FRET effect was observed when FRET micelles were dispersed in deionized water. Thus, the prepared FRET micelles could be used to measure the FRET effect to monitor the encapsulation of the core-loaded molecules in micelles.

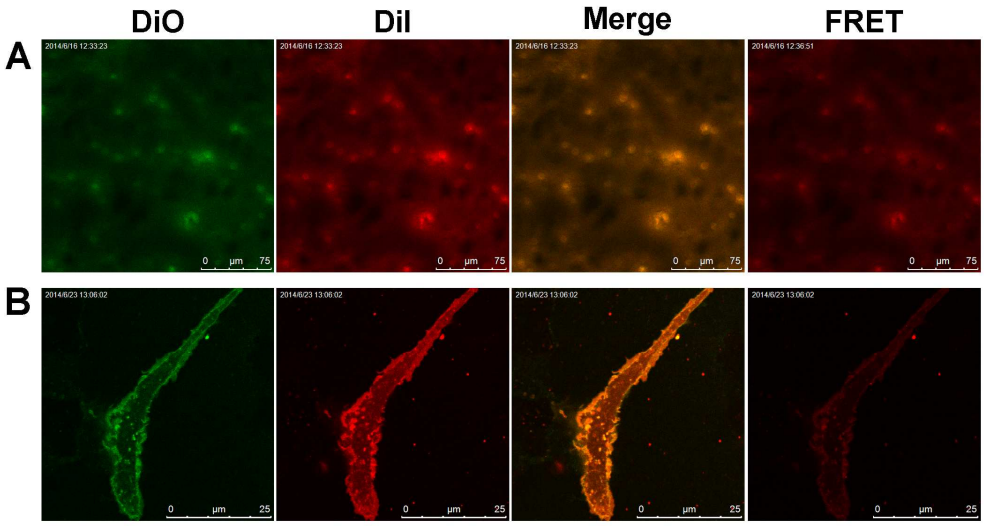

Fig.3 (A) Confocal images of (DiO/DiI)-loaded PEOz-PLA micelles in deionized water. (B) FRET analysis of (DiO/DiI)-loaded PEOz-PLA micelles when they contacted with 22Rv1 cells for 1 h. The Ex/Em of the DiO and DiI lines was DiO/DiO, DiI/DiI (484/501, 549/565). The Ex/Em of the FRET line was DiO/DiI (484/565). The merge line represents the fluorescence intensity.

A strong FRET effect was also observed after FRET micelles incubated with 22Rv1 cells for 1h (Fig.3B) although the micelles might escape from eddo/lysosomes and the core-loaded agents released from micelles as described below, possibly due to dynamic cellular uptake process of the micelles. This implied that intracellular FRET effect still existed after the micelles were internalized by cells, evidencing the encapsulation of lipophilic agent in the inner core of the micelles up on cellular uptake. It appeared that intact polymeric micelles were taken into cells, followed by intracellular release of FRET pair.[33] Thus, the behavior of loaded C6 was considered representative of the behavior of micelles after they contacted with cells.

3.5 In vitro cytotoxicity

Biocompatibility is a great concern for biomaterials, and in this study a preliminary evaluation of cytotoxicity of the blank micelles was performed using SRB assay. PC-3 and 22Rv1 cells were chosen for this study because PC-3 cells are PSMA-negative cells and 22Rv1 cells are PSMA-positive cells. A relative cell viability of around 100% was observed for PC-3 (Fig.4A) and 22Rv1 (Fig.4B) cells up to the highest polymer concentration of 10 mg/mL, and no significant change was detected in cell viability with increasing of copolymer concentration (p>0.05). These suggested that neither HOOC-PEOz-PLA copolymer itself nor its hydrolytic products exhibited cytotoxicity substantially. Eventually, HOOC-PEOz-PLA prepared in the present study was biocompatible, and was a good micelle-forming biomaterial for drug delivery.

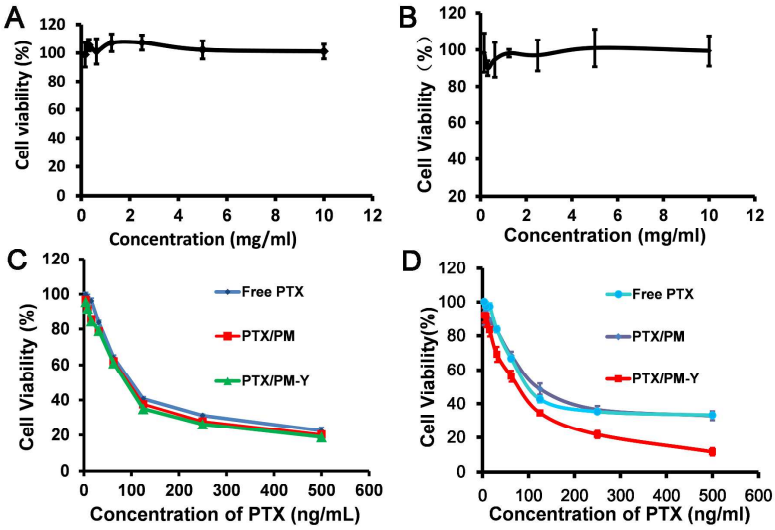

Fig.4 Cytotoxicity of blank micelles against PC-3 (A) and 22Rv1 cells (B), and various PTX-loaded micelles against PC-3 (C) and 22Rv1 cells (D) after incubation for 72h (*n*=6).

To apply PTX-loaded micelles for *in vivo* tumor therapy, their inhibiting effect on the growth of tumor cells (PC-3 and 22Rv1) was quantitatively evaluated *in vitro*, and the IC_{50} value (the drug concentration at which 50% of cells are killed) was calculated simultaneously. Apparent inhibition on the two cell lines was observed in a concentration-dependent pattern (Fig.4C and Fig.4D). Free PTX could be internalized easily and accumulated in cells at high level, thus leading to high cytotoxicity, and the encapsulation of PTX into unmodified micelles (i.e., PTX/PM) resulted in no obvious increase in the cytotoxicity of PTX compared with free PTX (Table 2). For PC-3 cells (Fig.4C), a PSMA-negative cell line, PTX/PM-Y resulted in no obvious increase in cytotoxicity of PTX compared with PTX/PM (Fig.4C and Table 2). In contrast, for 22Rv1 cells (Fig.4D), a PSMA-positive cell line, apparent cell growth inhibition was observed in a formulation-dependent pattern. The growth of tumor cells was severely inhibited after

incubation with PTX/PM-Y for 72 h compared with that of PTX/PM. The IC_{50} value of PTX/PM-Y was 1.10-fold lower than that of PTX/PM, suggesting that the conjugation of YPSMA-1 to the surface of PTX/PM could increase the cytotoxicity of PTX. This superior cytotoxicity of PTX/PM-Y against 22Rv1 cells might be attributed to the effect of YPSMA-1 receptor targeting.

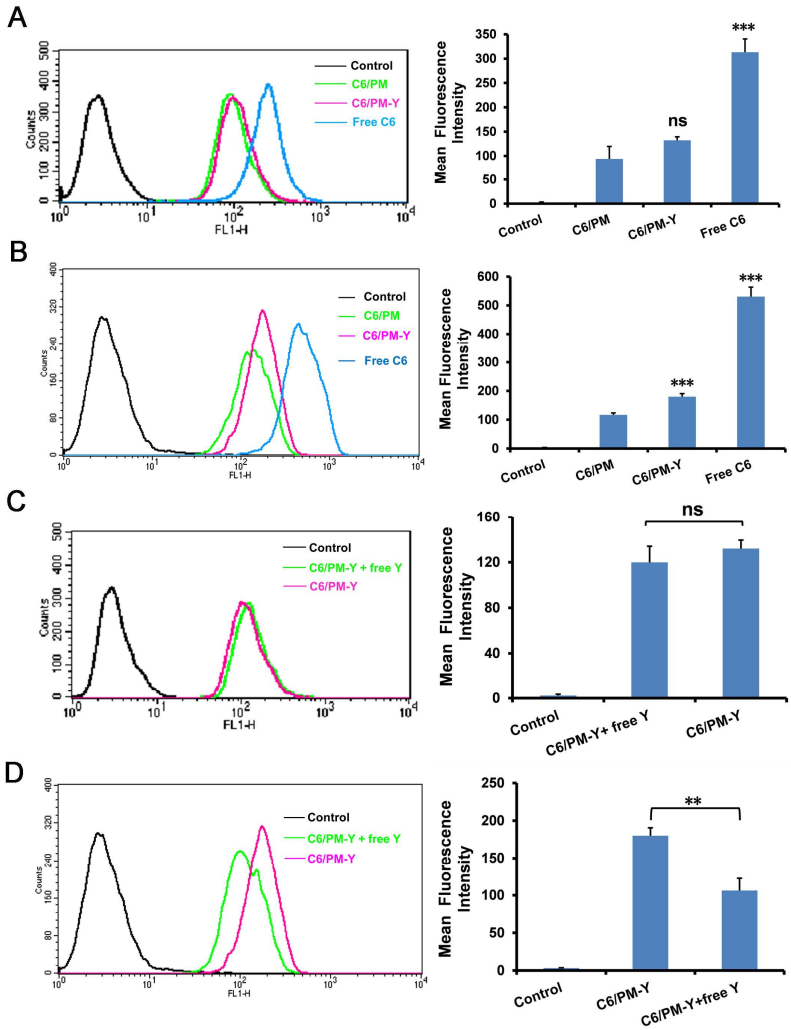

Fig.5 Quantitative flow cytometry analysis results of C6 uptake from various C6-loaded micelles by PC-3 (A) and 22Rv1 (B) cells after 4 h incubation. The competitive inhibition of free YPSMA-1 on C6 uptake by preincubation with 0.1 μg/mL of free YPSMA-1 for 30 min before PC-3 cells (C) and 22Rv1 cells (D) were exposed to the corresponding micelles.

$^{**}p<0.01$, $^{***}p<0.001$, ^{ns} $p>0.05$ compared with the respective control. The final C6 concentration in each formulation was 100 ng/mL.

3.6 In vitro cellular uptake

Flow cytometry was first utilized to quantitatively evaluate the cellular uptake of various micelles by tumor cells. C6 was employed as the marker for intracellular tracing. For PC-3 cells (Fig.5A), there was no significant difference in fluorescence intensity of C6 for C6/PM-Y and C6/PM ($p>0.05$). In comparison, for 22Rv1 cells (Fig.5B), C6/PM-Y significantly increased the cellular uptake of C6 compared with C6/PM ($p<0.001$), and the intracellular fluorescence intensity for C6/PM-Y was 1.55-fold higher than that for C6/PM. This result indicated that YPSMA-1 decorated on the micelle surface considerably enhanced the cellular uptake of C6/PM-Y by 22Rv1 cells, which might be attributed to PSMA-mediated endocytosis.

In order to verify the hypothesis of the promotion of the cellular uptake of C6/PM-Y by YPSMA-1 conjugated on the surface of micelles, the competitive inhibition of free YPSMA-1 was assayed by incubation of free YPSMA-1 with cells in advance (Fig.5C and Fig.5D). The cellular uptake of C6/PM-Y was significantly reduced in PSMA-positive 22Rv1 cells ($p<0.01$) (Fig.5D), while there was no significant change in PSMA-negative PC-3 cells ($p>0.05$) (Fig.5C), confirming that the increase in cellular uptake of C6/PM-Y by 22Rv1 cells mainly resulted from the mediation of PSMA.

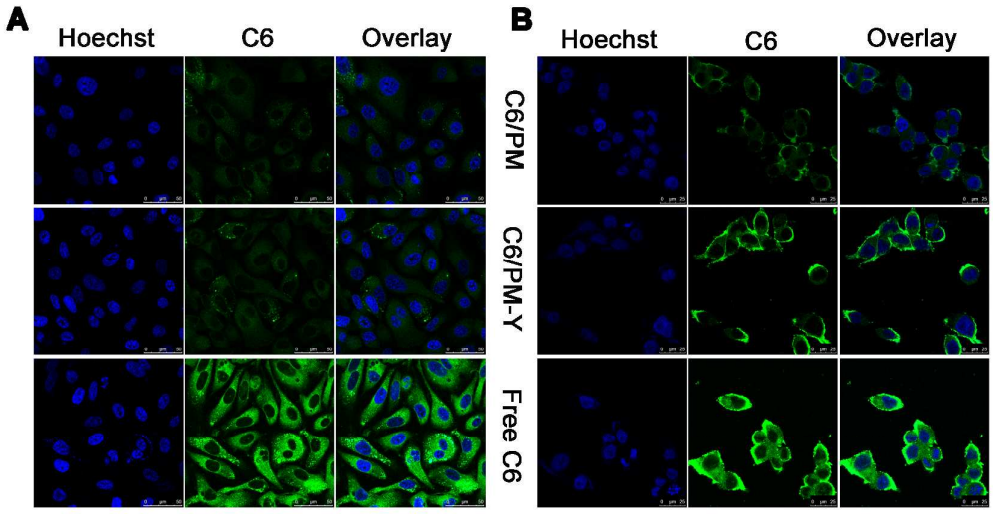

Fig.6 Confocal microscopy images of PC-3 (A) and 22Rv1 (B) cells incubated with various C6 formulations at 37°C for 1 h and 1.5 h, respectively. The final C6 concentration in each formulation was 50 ng/mL. Cell nuclei were stained blue with Hoechst 33258, and green fluorescence is from C6 encapsulated in micelles.

The cellular uptake was further visualized by CLSM to qualitatively evaluate the amount of micelles endocytosed by tumor cells and intracellular distribution using C6 as fluorescent probe. After being incubated with various C6 formulations for 1 h (PC-3 cells) and 1.5 h (22Rv1 cells), respectively, tumor cells were fixed and stained with Hoechst 33258 to reveal their cell nuclei morphology *in vitro*. Fig.6 presented the intracellular accumulation and distribution of various C6 formulations in PC-3 (Fig.6A) and 22Rv1 (Fig.6B) cells. Because of its higher hydrophobicity, free C6 readily partitioned into the lipid membranes, thus leading to the most intense intracellular green fluorescence, and free C6 was mainly located in the cytoplasm. Further, the two micelles did not show nuclear delivery and accumulated C6 with green fluorescence in the cytoplasm. For

C6/PM-Y, the fluorescence intensity of C6 in PC-3 cells was similar to that of C6/PM (Fig.6A); however, the intense fluorescence of C6 for C6/PM-Y in 22Rv1 cells was more marked than that for C6/PM (Fig.6B). Overall, the intracellular green fluorescence intensity ranked as free C6 > C6/PM-Y≈C6/PM for PC-3 cells, and free C6 > C6/PM-Y > C6/PM for 22Rv1 cells. Stronger fluorescent signals indicated higher internalization of C6. These results supported our cellular uptake studies by flow cytometry.

3.7 Tracking of endo/lysosome escape of micelles

As known, different properties of micelles will influence their intracellular trafficking pathway, which can influence their final fate and thereby therapy efficacy.[34] Thus, understanding the intracellular trafficking of micelles is necessary for obtaining their properties. Towards this, C6 with green fluorescence and LysoTracker red were used to label micelles and endo/lysosomes, respectively, to observe the distribution of micelles in tumor cells by CLSM, while non-responsive mPEG-PLA micelles were selected as control for comparison. Here, PC-3 cells were selected as model tumor cells due to their ease of culture. As shown in Fig.7, the vivid green color (C6 labeled micelles) was highly luminescent with red colors (LysoTracker red stained endo/lysosomes) in cells incubated with both C6/PM and C6/mPEG-PLA micelles for different time intervals. Specifically, a large portion of the two micelles were accumulated in endo/lysosomes at 0 h, while the colocalization of C6/PM with endo/lysosomes was obviously lower than that of C6/mPEG-PLA micelles at 0.5 h, 1 h and 3 h. In addition, C6/mPEG-PLA micelles presented no statistically significant difference in colocalization with endo/lysosomes during the test period (p>0.05) (Fig.7A and Fig. 7C). These implied that C6/PM exhibited a

better ability of endo/lysosome escape, but C6/mPEG-PLA micelles still stayed in endo/lysosomal vesicles during the test period.

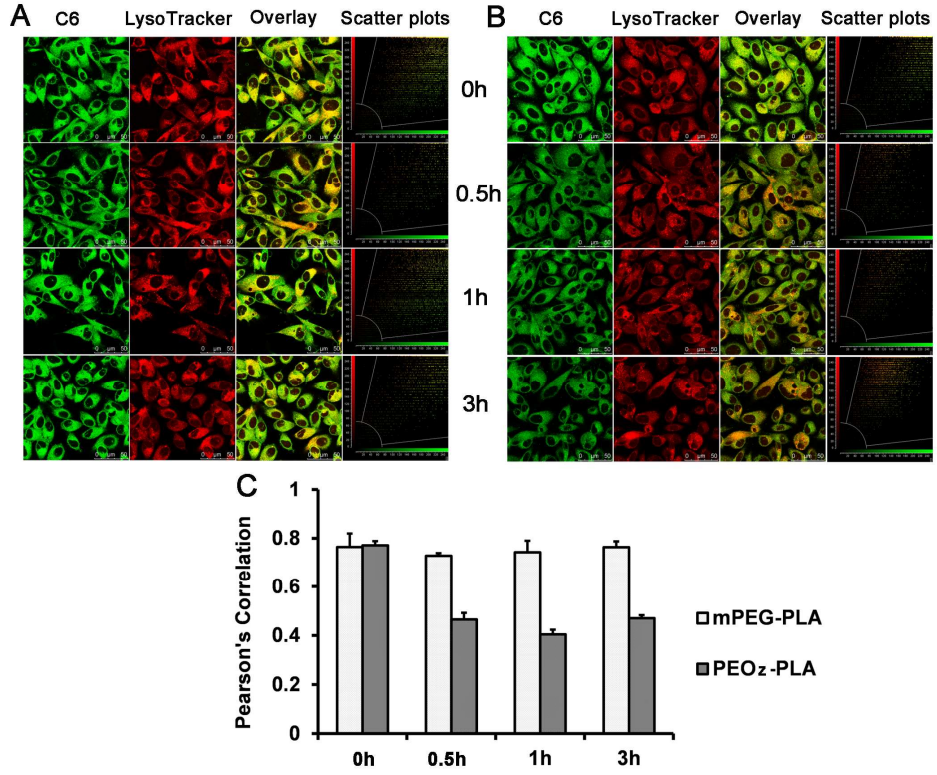

Fig.7 CLSM images of colocalization of C6/mPEG-PLA micelles (A) and C6/PM (B) with endo/lysosomes in PC-3 cells at different time points. Green fluorescence is from C6 encapsulated in the two micelles. Red fluorescence is from LysoTracker® Red stained endo/lysosomes. Yellow color is an indication for localization of C6 (green) in endo/lysosomes (red). (C) Quantitative colocalization analysis of micelles with endo/lysosomes using LAS AF.

Further, the colocalization of C6/PM with endo/lysosomes at 0 h was obviously higher than that at 0.5 h, 1 h and 3 h, respectively, and no statistically significant difference in colocalization was detected after 0.5 h (p>0.05). More importantly, the

Person's correlation of C6/PM was below 0.5 at 0.5 h, 1 h and 3 h (Fig.7C). These suggested that a great portion of C6/PM efficiently escaped from endo/lysosomes before 0.5 h, which contributed to avoid the degradation of cargos by lysosomes.

3.8 Real-time tracing intracellular trafficking of micelles

The real-time observation of colocalization of nanoparticles with intracellular organelles facilitates us to better understand their intracellular trafficking process. Thus, the colocalization of our prepared pH-sensitive micelles with endosomes and lysosomes in living cells was examined, for the first time, over time using real-time CLSM, respectively. Towards this, PC-3 cells were selected as model tumor cells due to their ease of culture.

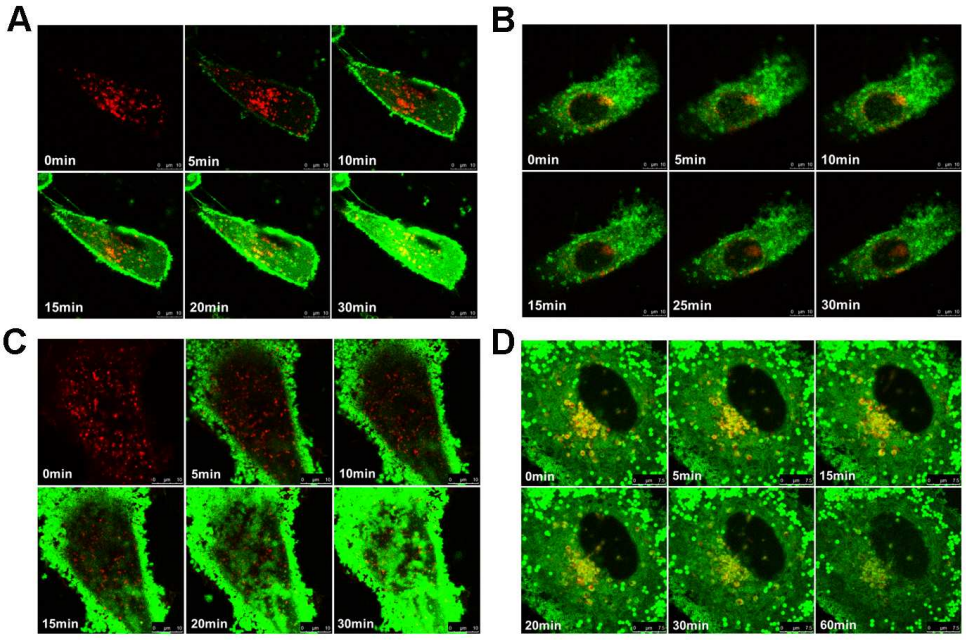

Fig.8 CLSM images in real-time tracing intracellular trafficking of C6/PM in PC-3 cells. The internalization kinetics of the micelles by endosomes (A) and lysosomes (C). The escape kinetics of the micelles from endosomes (B) and lysosomes (D). Green

fluorescence is from C6/PM. Red fluorescence is from CellLight® Endosome-RFP Red stained endosomes or Lysosome-RFP Red stained lysosomes. Yellow color is an indication for localization of C6 (green) in endosomes or lysosomes (red). Image frames were extracted from videos for comparison.

After 24 h transfection with the fluorescent fusion proteins, endosomes and lysosomes labeled PC-3 cells were incubated with C6/PM and imaged for 30 min or 60 min, respectively. Fig.8A and Fig.8C presented a series of real-time CLSM images of C6/PM internalized by endosomes and lysosomes, respectively. It was evident that C6/PM was rapidly and effectively internalized into cells and the green fluorescence intensity increased with increased incubation time. Specifically, when C6/PM was added to endosomes labeled cell suspension (0 min), there was no fluorescence recorded because the fluorescence of C6/PM outside cells was invisible under CLSM (Fig.8A). At about 5 min, more C6/PMs were internalized into cells, which was judged by the green fluorescence. The colocalization of C6/PM with endosomes, indicated by the yellow fluorescence in merged image due to the overlap of C6/PM (green) and CellLight® Endosome-RFP red stained endosomes (red), was initially seen at about 10 min, demonstrating that C6/PM was not mainly located in endosomes before then. Thereafter, more and more C6/PM was captured by endosomes as time increased, which was evidenced by the increased yellow fluorescence. In contrast, as for the colocalization of C6/PM with lysosomes (Fig.8C), a marginally yellow fluorescence was observed until 20 min. Afterwards, more and more micelles colocalized with lysosomes, however, the image

exhibited lower yellow fluorescence in lysosomes labeled cells than endosomes labeled cells, suggesting that some of C6/PMs escaped from endosomes during the view period.

Fig.8B and Fig.8D showed the escape process of C6/PM from endosomes and lysosomes after the cells were washed with blank culture medium, respectively. It was obvious that the micelles gradually escaped from endosomes with the time increased, evidenced by the decreased yellow fluorescence, and no yellow fluorescence was observed from 15 min to the end of the test (Fig.8B). In comparison, for lysosome labeled cells (Fig.8D), the vivid yellow color was highly luminescent with green colors (C6/PM) in cells during the first 15 min. Similar to the case of endosome escape, the yellow fluorescence decreased during the test period. At the end of the observation, almost all the micelles escaped from lysosomes. These findings provided, for the first time, the direct evidence that a fraction of micelles escaped from endosomes, thereby bypassing the degradative lysosomes pathway, and the other was delivered to lysosomes and escaped later.

3.9 In vivo antitumor efficacy

In vivo antitumor efficacy of various PTX-loaded micelles was finally estimated in PC-3 and 22Rv1 xenograft-bearing mice, respectively. The tumor size at fixed time intervals was measured in order to quantitatively evaluate the tumor growth after injection of various PTX formulations. The growth curves of tumors were shown in Fig.9A and Fig. 9B. Notably, as compared with the control group of saline (negative), the volume of tumors treated with various PTX formulations reduced continuously after the second treatment, suggesting that all PTX formulations exhibited considerable tumor suppression activity. As

anticipated, all the PTX-loaded micelles possessed better antitumor efficacy compared with the positive control group (Taxol®).

For PC-3 xenograft-bearing mice (Fig.9A), the inhibitory effect of tumor growth by PTX/PM-Y was comparable to that by PTX/PM (p>0.05), which was also evidenced by the images of the tumor mass excised from the xonegraft model on the day 12 after treatments (Fig.9C). The PTX/PM and PTX/PM-Y treatment groups showed the smallest tumor mass, followed by Taxol®, in increasing order of volume.

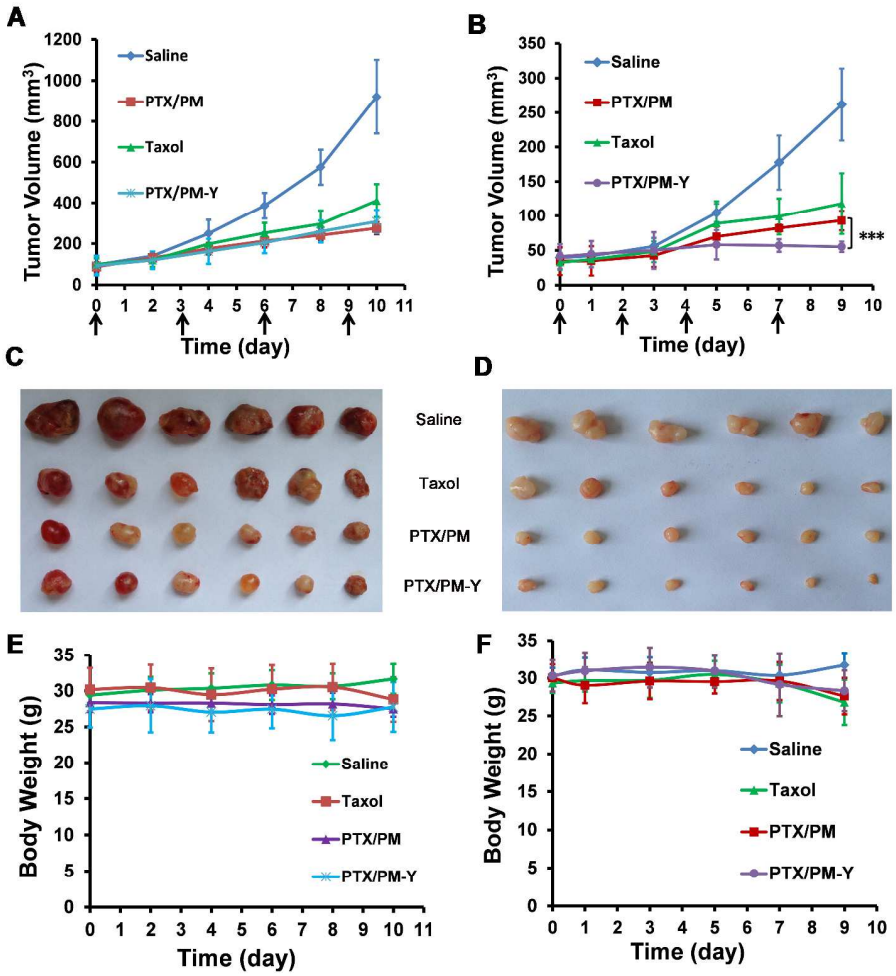

Fig.9 Tumor suppression at the whole-body level. (A and B) Changes of tumor volume after intravenous injection of saline, Taxol®, PTX/PM, and PTX/PM-Y in PC-3 (A) and

22Rv1 (B) tumor-bearing nude mice. The arrows indicated injection time points. (C and D) PC-3 (C) and 22Rv1 (D) tumor mass from each treatment group excised on day 12 for PC-3 xenograft-bearing mice or day 10 for 22Rv1 xenograft-bearing mice after treatments. (E and F) Body weight changes of PC-3 (E) and 22Rv1 (F) tumor-bearing mice after treatments (n=6). ***p< 0.001.

For 22Rv1 xenograft-bearing mice (Fig.9B), PTX/PM-Y was more effective in preventing tumor growth than PTX/PM (p<0.001). This result once again revealed that the modification of the micelles by YPSMA-1 enhanced the antitumor effect *in vivo*, which might be assigned to the PSMA-mediated active targeting. This was also supported by the images of the final tumor mass excised from the xonegraft model (Fig.9D).

Body weight changes of mice, as an indicator of systemic toxicity, were monitored periodically following administration. As shown in Fig.9E and Fig.9F, just like saline treated mice, body weight for all the micelles treated mice did not change greatly, demonstrating a good biocompatibility of our prepared polymeric micelles. However, severe weight loss was observed after the last treatment for Taxol® treated group, indicating the serious systematic toxicity of Taxol®.

4 Discussion

Formulating drugs to bind to the desired cellular targets is a necessary step in the design of anticancer drug delivery systems.[35, 36] Further, following internalization, it is desirable to protect drugs from the degradation in the acidic lysosomes by lysosomal enzymes.[19, 37] Introducing pH-sensitive moieties into the targeting drug delivery systems

were expected to achieve precise targetability and enhanced cellular internalization,[38, 39] and quick endo/lysosome escape.[40] Here, we developed novel PSMA-mediated pH-sensitive polymeric micelles for targeted delivery of PTX to tumors and explored their therapeutic efficiencies for prostate cancer.

First, the diblock copolymer HOOC-PEOz-PLA was successfully synthesized and selected as the main micelle-forming material, and its biocompatibility with negligible cell cytotoxicity was confirmed (Fig.4A and Fig.4B). The synthesized HOOC-PEOz-PLA could self-assemble into micelles with a small diameter and narrow distribution in aqueous medium and high drug loading capacity (Table 1). In addition, the combination of HOOC-PEOz-PLA with YPSMA-1-PEOz-PLA were engineered, which comprised the micelles for targeted delivery of PTX to tumor cells and controlled release triggered by endocytic pH after being internalized into tumor cells via endocytosis and trapped in acidic endocytic compartments, thus the toxicity of encapsulated PTX is made more tumor cell-specific and enhanced.[39] As expected, all the designed micelles in the present study distinguished endo/lysosomal pH from physiological pH by accelerating drug release (Fig.2C and Fig.2D). This pH-dependent release was attributed to the stronger protonation of the tertiary amide groups in PEOz located in the outer shell of the micelles at endo/lysosomal pH, thereby inducing intermolecular interactions through hydrogen bond amongst micelles that may have caused collapse of the micelle outer shell.[41] In addition, the charge density of the micelle surface increased due to the ionization of PEOz at endo/lysosomal pH, thus the increased electrostatic repulsion between PEOz blocks induced the loose micelle structure (Scheme 1A).[42] Based on the *in vitro* release results, it

could be concluded that after internalization of the micelles, pH-triggered drug release at endo/lysosomal pH, which resulted in the “proton-sponge effect” and further led to the rupture of endo/lysosome membrane,[43] could facilitate the escape of the micelles and their payload from endo/lysosomes. This was further supported by a pronounced distinction in intracellular localization viewed by CLSM in a time dependent manner between our designed micelles and non-responsive mPEG-PLA micelles (Fig.7). This pH-triggered quick drug release might remarkably enhance the intracellular free drug concentration in a short time,[1, 44] being beneficial to kill tumor cells and shrink tumors [41] and possibly deterring the occurrence of drug resistance for tumor cells, which will be confirmed in the future study. Additionally, the present findings obtained by *in vivo* antitumor efficacy studies (Fig.9) further demonstrated that pH-sensitivity endowed the micelles (PTX/PM) with passive tumor targeting effect,[2, 45] which was assigned to the fact that the lower pH in the tumor extracellular matrix provides a tissue-specific stimulus.[46]

To date, despite the wide use of pH-responsive polymeric micelles for delivery of antitumor drugs to tumor cells, their intracellular trafficking pathway is not yet clarified. Previous studies demonstrated that pH-responsive polymeric micelles could rapidly escape from endo-lysosomes,[34,40] which was evidenced by CLSM images of subcellular colocalization of fluorescence labeled micelles with acidic organelles, both endosomes and lysosomes, stained by LysoTracker Red, a specific marker for these acidic organelles. No study on observing the intracellular trafficking of pH-responsive micelles by separately labeling endosomes and lysosomes has yet been reported, and whether pH-sensitive micelles avoid lysosomal pathway completely has remained unclear. Furthermore,

understanding of the intracellular trafficking pathway is critically important for designing a desirable micelle delivery system. Therefore, we paid particular attention to this for our designed micelles. Real-time and in situ CLSM imaging provided, for the first time, the direct evidence that a large portion of pH-responsive C6/PM entrapped by endosomes after being internalized into cells quickly escaped from endosomes compared with plain micelles, thereby bypassing lysosomal pathway, and the residual was delivered into lysosomes and escaped eventually (Fig.8). These results suggested that PTX/PM would have better anticancer activity compared with non-responsive Taxol®, which was confirmed by the *in vivo* anticancer efficacy presented in Fig.9. On the other hand, this intracellular trafficking process implied that the uptake mechanism of our prepared micelles seemed to be relevant with clathrin-mediated endocytosis due to the fact that only clathrin-mediated endocytosis is characterized as endosome-lysosome pathway.[47] Moreover, our result demonstrated once more that the intracellular trafficking process of drug delivery systems depends on both their intrinsic properties and their endocytosis pathways in a given type of cells.[47, 48] Taken together, all these results confirmed that our designed micelles could be endocytosed by tumor cells and then quickly released PTX into cytoplasm triggered by endo/lysosomal pH. Finally, the released PTX initiated its action to induce apoptosis and cell death.

For effective cancer treatment, anticancer drug must be accumulated in tumors. One of the rational and effective strategies is to deliver drug to tumor cells using targeting ligand-modified nanocarriers.[6, 15, 49-54] The present study further suggested the benefit of using ligand-modified pH-sensitive micelles for enhanced targeting ability and

receptor-mediated cellular uptake.[38, 39] The results of cellular uptake (Fig.5 and Fig.6), *in vitro* and *in vivo* antitumor efficacy (Fig.4 and Fig.9) provided incontrovertible evidences of targeting effect of YPSMA-1-modified micelles to PSMA-positive 22Rv1 tumor cells. Additionally, targetability and pH-sensitivity could provide a synergistic effect. *In vivo* antitumor efficacy (Fig.9) results confirmed such combined effect of PEOz-PLA induced pH-sensitivity with receptor mediated endocytosis.[39] Nevertheless, further studies regarding *in vivo* distribution and pharmaceutic kinetics of the prepared micelles will be carried out to fully characterize their *in vivo* nature. Overall, these results strongly supported our hypothesis that the combination of pH-sensitivity with YPSMA-1-modification in polymeric micelles enhanced tumor cell recognition, promoted the cellular uptake, facilitated their cargos to escape from endo/lysosomes, thereby improving the antitumor efficacy. The design concept in this study might provide a reference to the delivery of antitumor agents for safe and effective therapy of PSMA-positive prostate cancers.

5 Conclusions

In summary, we designed and fabricated PTX-loaded pH-sensitive polymeric micelles modified with YPSMA-1 to combine active targeting to PSMA-positive prostate cancer cells with fast intracellular release of drug. It was demonstrated that YPSMA-1-modified micelles had excellent performance featured by nano-scaled size to obtain EPR effect, favorable pH-sensitivity to promote endo/lysosome escape and rapid drug release to kill tumor cells with effective concentration, higher PSMA-binding affinity to enhance targeting to PSMA-positive tumor cells, leading to enhanced cellular uptake and cytotoxicity and

thereby therapeutic efficacy of prostate cancers with negligible systemic toxicity. These suggested that PSMA-mediated pH-sensitive polymeric micelle delivery system might be a powerful drug carrier for targeting therapy of PSMA-positive prostate cancers.

Acknowledgements

This work was financially supported by the National Natural Science Foundation of China (No. 81172990), the National Key Science Research Program of China (973 Program, 2015CB932100) and the Innovation Team of Ministry of Education (No. BMU20110263).

Notes and references

1 C. Cui, Y.N. Xue, M. Wu, Y. Zhang, P. Yu, L. Liu, R.X. Zhuo, S.W. Huang, *Biomaterials*, 2013, 34, 3858-3869.

2 M. Talelli, M. Iman, A.K. Varkouhi, C.J. Rijcken, R.M. Schiffelers, T. Etrych, K. Ulbrich, C.F. van Nostrum, T. Lammers, G. Storm, W.E. Hennink, Biomaterials, 2010, 31, 7797-7804.

3 X. Yang, J.J. Grailer, S. Pilla, D.A. Steeber, S. Gong, *Bioconjug. Chem.*, 2010, 21, 496-504.

4 X.B. Xiong, A. Lavasanifar, *ACS Nano*, 2011, 5, 5202-5213.

5 I.F. Tannock, R. de Wit, W.R. Berry, J. Horti, A. Pluzanska, K.N. Chi, S. Oudard , C. Théodore, N.D. James, I. Turesson, M.A. Rosenthal, M.A. Eisenberger, *N. Engl. J. Med*., 2004, 351, 1502-1512.

6 Y. Chen, G. Wang, D. Kong, Z. Zhang, K. Yang, R. Liu, W. Zhao, Y. Xu, *Mol. Carcinog.,* 2013, 52, 237-246.

7 S.S. Chang, *Curr. Opin. Invest. Drugs*, 2004, 5, 611-615.

8 A.K. Iyer, G. Khaled, J. Fang, H. Maeda, *Drug Discov. Today*, 2006, 11, 812-818.

9 T.M. Allen, *Nat. Rev. Cancer*, 2002, 2, 750-763.

10 S.M. Hillier, A.M. Kern, K.P. Maresca, J.C. Marquis, W.C. Eckelman, J.L. Joyal, J.W. Babich, *J. Nucl. Med*., 2011, 52, 1087-1093.

11 S. Ikegami, K. Yamakami, T. Ono, M. Sato, S. Suzuki, I. Yoshimura, T. Asano, M. Hayakawa, T. Tadakuma, *Hum. Gene Ther*., 2006, 17, 997-1005.

12 D.J. Bacich, J.T. Pinto, W.P. Tong, W.D. Heston, *Mamm. Genome*, 2001, 12, 117-123.

13 G.L. Wright Jr., B.M. Grob, C. Haley, K. Grossman, K. Newhall, D. Petrylak, J. Troyer, A. Konchuba, P.F. Schellhammer, R. Moriarty, *Urology*, 1996, 48, 326-334.

14 S.F. Slovin, *Expert Opin. Ther. Targets*, 2005, 9, 561-570.

15 R.M. Sawant, M.B. Cohen, V.P. Torchilin, O.W. Rokhlin, *J. Drug Target.*, 2008, 16, 601-604.

16 T.W. Hambley, W.N. Hait, *Cancer Res*., 2009, 69, 1259-1262.

17 V. Torchilin, *Eur. J. Pharm. Biopharm*., 2009, 71, 431-444.

18 A. Klaikherd, C. Nagamani, S. Thayumanavan, J. Am. Chem. Soc., 2009, 131, 4830-4838.

19 K. Sakai-Kato, K. Un, K. Nanjo, N. Nishiyama, H. Kusuhara, K. Kataoka, T. Kawanishi, Y. Goda, H.

Okuda, *Biomaterials,* 2014, 35, 1347-1358.

20 D. Kim, E.S. Lee, K.T. Oh, Z.G. Gao, Y.H. Bae, *Small*, 2008, 4, 2043-2050.

21 D. Kim, Z.G. Gao, E.S. Lee, Y.H. Bae, *Mol. Pharm*., 2009, 6, 1353-1362.

22 Y. Zhang, X. Li, Y. Zhou, Y. Fan, X. Wang, Y. Huang, Y. Liu, *Mol. Pharm*., 2010, 7, 1169-1182.

23 S. Zalipsky, C.B. Hansen, J.M. Oaks, T.M. Allen, *J. Pharm. Sci*., 1996, 85, 133-137.

24 X. Wang, X. Li, Y. Li, Y. Zhou, C. Fan, W. Li, S. Ma, Y. Fan, Y. Huang, N. Li, Y. Liu, *Acta Biomater*., 2011, 7, 4149-4159.

25 X. Li, Z. Yang, K. Yang, Y. Zhou, X. Chen, Y. Zhang, F. Wang, Y. Liu, L. Ren, *Nanoscale Res. Lett*., 2009, 4, 1502-1511.

26 X. Li, P. Li, Y. Zhang, Y. Zhou, X. Chen, Y. Huang, Y. Liu, *Pharm. Res*., 2010, 27, 1498-1511.

27 H. Chen, S. Kim, L. Li, S. Wang, K. Park, J.X. Cheng, *Proc. Natl. Acad. Sci. U. S. A.*, 2008, 105, 6596-6601.

28 N, Li, X.R. Li, Y.X. Zhou, W.J. Li, Y. Zhao, S.J. Ma, J.W. Li, Y.J. Gao, Y. Liu, X.L. Wang, D.D. Yin, *Biomaterials*, 2012, 33, 8881-8892.

29 V. Zinchuk, O. Grossenbacher-Zinchuk, *Prog. Histochem. Cytochem*., 2009, 44, 125-172.

30 X. Duan, Y. Li, *Small*, 2013, 9, 1521-1532.

31 H. Maeda, Y. Matsumura, *Crit. Rev. Ther. Drug Carrier Syst*., 1989, 6, 193-210.

32 Z.G. Gao, A.N. Lukyanov, A. Singhal, V.P. Torchilin, *Nano Lett*., 2002, 2, 979-982.

33 J.A. Hubbell, *Science*, 2003, 300, 595-596.

34 P. Liu, Y. Sun, Q. Wang, Y. Sun, H. Li, Y. Duan, *Biomaterials*, 2014, 35, 760-770.

35 C. Liu, F. Liu, L. Feng, M. Li, J. Zhang, N. Zhang, *Biomaterials*, 2013, 34, 2547-2564.

36 Y. Xiao, H. Hong, A. Javadi, J.W. Engle, W. Xu, Y. Yang, Y. Zhang, T.E. Barnhart, W. Cai, S. Gong, *Biomaterials,* 2012, 33, 3071-3082.

37 H.Y. Nam, S.M. Kwon, H. Chung, S.Y. Lee, S.H. Kwon, H. Jeon, Y. Kim, J.H. Park, J. Kim , S. Her, Y.K. Oh, I.C. Kwon, K. Kim, S.Y. Jeong, *J. Control. Release*, 2009, 135, 259-267.

38 G.H. Hsiue, C.H. Wang, C.L. Lo, C.H. Wang, J.P. Li, J.L .Yang, *Int. J. Pharm*., 2006, 317, 69-75.

39 H. Wu, L. Zhu, V.P. Torchilin, *Biomaterials*, 2013, 34, 1213-1222.

40 M. Wang, H. Hu, Y. Sun, L. Qiu, J. Zhang, G. Guan, X. Zhao, M. Qiao, L. Cheng, L. Cheng, D. Chen, *Biomaterials,* 2013, 34, 10120-10132.

41 C.H. Wang, C.H. Wang, G.H. Hsiue, *J. Control. Release,* 2005, 108, 140-149.

42 C.Y. Zhang, Y.Q. Yang, T.X. Huang, B. Zhao, X.D. Guo, J.F. Wang, L.G. Zhang, *Biomaterials,* 2012, 33, 6273-6283.

43 Y. Hu, T. Litwin, A.R. Nagaraja, B. Kwong, J. Katz, N. Watson, D.J. Irvine, *Nano Lett.*, 2007, 7, 3056-3064.

44 G.K. Xu, X.Q. Feng, B. Li, H. Gao, *J. Phys. Chem. B*, 2012, 116, 6003-6009.

45 W. Xu, I.A. Siddiqui, M. Nihal, S. Pilla, K. Rosenthal, H. Mukhtar, S. Gong, *Biomaterials*, 2013, 34, 5244-5253.

46 R. van Sluis, Z.M. Bhujwalla, N. Raghunand, P. Ballesteros, J. Alvarez, S. Cerdan, J.P. Galons, R.J. Gillies, *Magn. Reson. Med*., 1999, 41, 743-750.

47 S. Xiang, H. Tong, Q. Shi, J.C. Fernandes, T. Jin, K. Dai, X. Zhang, *J. Control. Release*, 2012, 158, 371-378.

48 J. Rejman, A. Bragonzi, M. Conese, *Mol. Ther*.,. 2005, 12, 468-474.

49 J. Cheng, B.A. Teply, I. Sherifi, J. Sung, G. Luther, F.X. Gu, E. Levy-Nissenbaum, A.F. Radovic-Moreno, R. Langer, O.C. Farokhzad, *Biomaterials*, 2007, 28, 869-876.

50 N.H. Bander, D.M. Nanus, M.I. Milowsky, L. Kostakoglu, S. Vallabahajosula, S.J. Goldsmith, *Semin. Oncol*., 2003, 30, 667-676.

51 X. Jiang, X. Sha, H. Xin, L. Chen, X. Gao, X. Wang, K. Law, J. Gu, Y. Chen, Y. Jiang, X. Ren, Q. Ren, X. F ang, *Biomaterials*, 2011, 32, 9457-9469.

52 C. Zhan, B. Gu, C. Xie, J. Li, Y. Liu, W. Lu, *J. Control. release*, 2010, 143, 136-142.

53 J.R. Nedrow-Byers, M. Jabbes, C. Jewett, T. Ganguly, H. He, T. Liu, P. Benny, J.N. Bryan, C.E. Berkman, *Prostate*., 2012, 72, 904-912.

54 S. Moffatt, R.J. Cristiano, *Int. J. Pharm*., 2006, 317, 10-13.